

Interaction of in-line twin synthetic jets with a separated flow

Cite as: Phys. Fluids **28**, 043602 (2016); <https://doi.org/10.1063/1.4946800>

Submitted: 07 January 2016 . Accepted: 03 April 2016 . Published Online: 20 April 2016

Xin Wen, Hui Tang , and Fei Duan



View Online



Export Citation



CrossMark

ARTICLES YOU MAY BE INTERESTED IN

[Vortex dynamics of in-line twin synthetic jets in a laminar boundary layer](#)

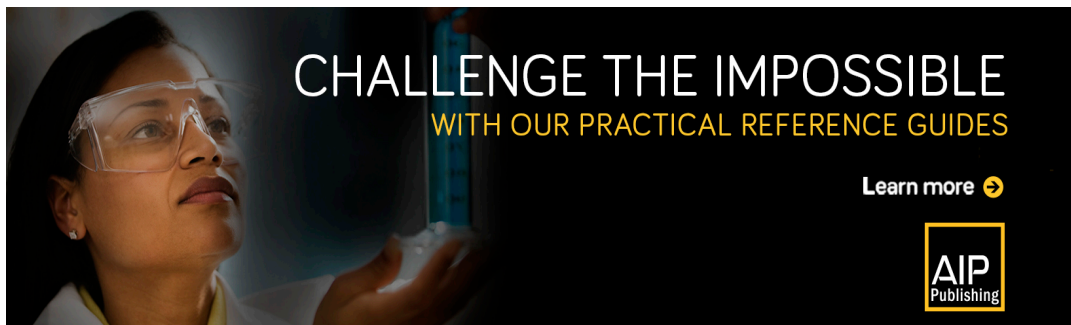
Physics of Fluids **27**, 083601 (2015); <https://doi.org/10.1063/1.4928216>

[Active control of vortex-induced vibrations of a circular cylinder using windward-suction- leeward-blowing actuation](#)

Physics of Fluids **28**, 053601 (2016); <https://doi.org/10.1063/1.4947246>

[Control of vortex-induced vibration using a pair of synthetic jets: Influence of active lock-on](#)

Physics of Fluids **29**, 083602 (2017); <https://doi.org/10.1063/1.4996231>



Interaction of in-line twin synthetic jets with a separated flow

Xin Wen,^{1,2} Hui Tang,^{3,a)} and Fei Duan¹

¹*School of Mechanical and Aerospace Engineering, Nanyang Technological University, Singapore 639798, Singapore*

²*Singapore-MIT Alliance for Research and Technology Center, Singapore 138602, Singapore*

³*Department of Mechanical Engineering, The Hong Kong Polytechnic University, Kowloon, Hong Kong, China*

(Received 7 January 2016; accepted 3 April 2016; published online 20 April 2016)

An experimental investigation is carried out in a water tunnel to investigate the interaction of in-line twin synthetic jets (SJs) with a separated laminar boundary layer over inclined plates. The flow structures induced by the in-line twin SJs at four phase differences and their resulting flow separation delay are examined using dye visualization and particle image velocimetry (PIV) measurements. It is found that, in most of the cases, the heads of hairpin vortices that are produced from the upstream SJ actuator do not change too much, and the vortex legs are highly stretched by the separated shear layer. An exception is the case with 90° phase difference where the combined vortex head appears as a reversed letter “S” and the combined vortex legs are high enough to escape from the influence of the separated flow. Compared to the single SJ, the twin SJs generally exert greater influence on the separated flow regardless of the phase difference. The PIV results in the mid-span plane reveal that the periodic passage of vortex structures influences the separated flow significantly, causing the flapping of the upper edge of the reversed flow region that contributes to the flow separation delay. The delay of separation is also demonstrated by a streak of forward flow protrusion in the wall-parallel PIV results. It is found that the streak varies a lot at different phase differences. Proper orthogonal decomposition analysis is also conducted and two major types of energetic flow structures in the SJ controlled flow are identified: a strip of back-and-forth fluctuation along the upper edge of the reversed flow, and the vortex structures produced by the twin SJs. It is found that the fluctuation strip is most energetic in the single SJ case and the case with 270° phase difference, whereas the convective mode pair is most energetic in the case with 90° phase difference. *Published by AIP Publishing.* [<http://dx.doi.org/10.1063/1.4946800>]

I. INTRODUCTION

Synthetic jet (SJ) has been demonstrated as a promising method for active flow control since 1990s due to its ability to inject momentum into ambient flows with zero net mass flux (Glezer and Amitay, 2002; Amitay and Glezer, 2002; Dandois *et al.*, 2007; Ibrahim and Skote, 2012; Tang *et al.*, 2014; and Wen and Tang, 2014). The control is usually accompanied by rich flow physics associated with the interaction between SJs and boundary layer flows. It is especially so for circular SJs, where the interaction is intrinsically three dimensional. When a circular SJ is perpendicularly issued into a turbulent boundary layer, Crook and Wood (2001) clearly observed using surface flow visualization that the SJ induced a pair of streamwise vortices, which extended downstream and interacted in a strongly three-dimensional manner with the separating boundary layer, causing

^{a)} Author to whom correspondence should be addressed. Electronic mail: h.tang@polyu.edu.hk

prominent delay of the separation. Using more advanced measurement technologies, the formation of counter-rotating vortex pairs after the injection of an isolate SJ into an attached boundary layer was observed in various studies (Zaman and Milanovic, 2003; Schaeffler and Jenkin, 2006; and Lai *et al.*, 2009). Furthermore, Jabbal and Zhong (2008) identified three types of SJ-induced vortex structures, namely, hairpin vortices, stretched vortex rings, and tilted/distorted vortex rings, under different crossflow and SJ operating conditions. By observing the thermal footprints of these vortex structures on a temperature-sensitive liquid crystal and their impact on the boundary layer velocity profiles, they conjectured that hairpin vortices and stretched vortex rings are more capable of energizing the boundary layer flow and hence delaying flow separation because they are closer to the wall (Jabbal and Zhong, 2010). The same group (Zhang and Zhong, 2010 and Zhong and Zhang, 2013) further confirmed that hairpin vortices induce a pair of streamwise vortices of opposite sign of rotation directly underneath, which plays a very important role in flow separation delay.

In many flow control applications, it is SJ arrays instead of isolated SJs that are commonly implemented (Crook and Wood, 2001; Amitay and Glezer, 2002; Zhong *et al.*, 2007; and Tang *et al.*, 2014). However, despite the success in laboratory applications, the detailed interaction among these SJs in boundary layers has not been fully understood. Only limited literature is available in this aspect. Using surface flow visualization, Watson *et al.* (2003) studied the interaction of in-phase twin SJs at various yaw angles relative to a boundary layer flow and found that the twin SJs interact in a constructive way when they are arranged in line with the ambient flow direction. Liddle *et al.* (2005) and Liddle and Wood (2005) then investigated the effect of phase difference between in-line twin SJs in a turbulent boundary layer using hotwire measurements, and revealed that although in most of the cases the dominant frequency in the controlled boundary layer coincides with the SJ operating frequency, at a special phase difference (happened to be 270°), it turns to a value twice of the SJ frequency, indicating that the flow structures induced by the twin SJs are completely separated and equispaced. In recent work on in-line twin SJs, Honami and Motosuke (2012) found that the vortex structures induced by the upstream SJ are able to maintain their coherence, whereas those induced by the downstream SJ are significantly affected by the upstream SJ and hence lose their coherence very easily.

With hairpin vortices produced, our recent investigations (Wen *et al.*, 2015 and Wen and Tang, 2016) on in-line twin SJs in an attached boundary layer revealed that three types of vortex structures can be induced under various operating phase differences: one combined vortex, two completely separated vortices, and partially interacting vortex structures. The one combined vortex is the strongest and is able to penetrate the boundary layer quickly. It can exert large spanwise influence on the near-wall flow. The two completely separated hairpin vortices stay low in the boundary layer and affect the near-wall flow in a narrow band along the mid-span plane. In the latter case, the dominant frequency in the controlled boundary layer is twice that of the SJ actuation frequency, similar to what was found by Liddle *et al.* (2005) and Liddle and Wood (2005).

Based on the good understanding achieved from the above investigations, in the present study, we go one step further to investigate the interaction of the same in-line twin SJs in a *separated* laminar boundary layer. Two research questions will be addressed: (1) What is the influence of the separated flow on the aforementioned three types of vortex structures? (2) To what extent these SJ-induced vortex structures can delay the flow separation? To facilitate this study, a water tunnel experiment is conducted on the same test rig used in our previous works, with a slight modification introduced. Both dye visualization and particle image velocimetry (PIV) measurements are implemented. In addition, proper orthogonal decomposition (POD) analysis is conducted to extract energy-carrying coherent structures in the interacting flow.

II. METHODOLOGY

A. Test rig

The present experimental investigation was conducted in a low-speed water tunnel with a test section of 1 m (L) \times 0.45 m (W) \times 0.45 m (H). The test rig is similar to that used in our previous studies on in-line twin SJs in an attached boundary layer (Wen *et al.*, 2015 and Wen and Tang, 2016).

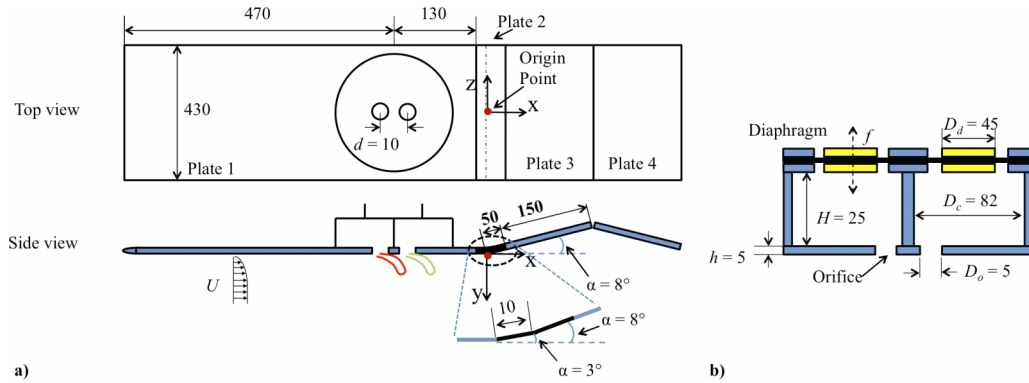


FIG. 1. Schematic of (a) the test plate and (b) the SJ actuators (not to scale, all dimensions are in mm).

But in the present study, a separated laminar flow was introduced to test the control effectiveness of the twin SJs at various conditions. Figure 1(a) shows a sketch of the test plate and its coordinate system. Most upstream located Plate 1 that is a horizontal plate of 600 mm long and equipped with a 1:5 elliptical leading edge. Plate 2 (shown in black in the side view) is a transitional plate of about 60 mm long that connects Plate 1 and Plate 3. It consists of two short upward inclined portions: the upstream one is about 10 mm long and inclined with a 3° angle to the horizontal plate, and the downstream one is about 50 mm long and introduces additional 5° inclination so that it is inclined with an 8° angle to the horizontal plate. The design of Plate 2 allows a smooth turn of the boundary layer flow developed over Plate 1. Plate 3 is a 150-mm-long plate that simply extends the downstream portion of Plate 2, which is also inclined with an 8° angle to the horizontal plate. With this set of plates, the boundary layer developed along the horizontal plate will separate at some point on Plate 2 or Plate 3, creating a flow separation region to which the in-line SJ based flow control will be applied. To prevent the occurrence of early separation on Plate 1, a 150-mm-long downward inclined plate, i.e., Plate 4, is attached to Plate 3, which is suggested in the work of Zhang and Zhong (2010). In addition, to minimize the possible disturbance caused by the gaps between connecting plates, waterproof paper of $50 \mu\text{m}$ thickness is used to cover these gaps. As shown in Fig. 1(a), the origin of the coordinate system used in the present study is set at the bending joint of Plate 2, with the x axis pointing to the freestream direction, the y axis pointing downward, and the z axis pointing to the spanwise direction.

Two SJ actuators are mounted on Plate 1, with their cavities located on the upper surface of the test plate and their orifices flush to the lower surface. As shown in the close-up view in Fig. 1(b), each SJ actuator has a cylindrical cavity with an orifice plate at its bottom side and an oscillating diaphragm clamped to its top side. The two orifices have the same diameter $D_o = 5$ mm and their center-to-center distance is fixed at $d = 10$ mm, i.e., $d/D_o = 2$. As indicated in Fig. 1(a), the centers of these two orifices are aligned in the boundary layer flow direction, and their midpoint is located at 470 mm downstream from the Plate 1's leading edge and is about 140 mm, i.e., $28D_o$, upstream of the origin of the current coordinate system. During the experiments, the oscillating diaphragms are driven by two permanent magnetic shakers, and the SJ actuator cavities are fully submerged in water. Further description of these two actuators can be found in our previous works (Wen *et al.*, 2015 and Wen and Tang, 2016).

B. Selection of test case

In the present study, the freestream velocity is fixed at $U_\infty = 0.11$ m/s. According to the boundary layer theory, a laminar boundary layer developed along the test plate shall have a thickness of about 10 mm ($2D_o$) and a momentum thickness based Reynolds number of about $Re_\theta = 150$ at the midpoint of the twin SJ actuators (i.e., $x = -28D_o$), and a thickness of about 12 mm ($2.4D_o$) and $Re_\theta = 170$ at the origin of the current coordinate system (i.e., $x = 0$). The SJ actuators operate with their diaphragm oscillating in a sinusoidal manner with a peak-to-peak displacement at $\Delta = 0.105$ mm and a frequency at $f = 2$ Hz. Under these conditions, the dimensionless stroke

length (i.e., the length of jet column in one period nondimensionalized by the orifice diameter) is $L = 1.7$ and the velocity ratio (i.e., ratio of the SJ velocity to the freestream velocity) is $VR = 0.16$. According to our previous works (Wen *et al.*, 2015 and Wen and Tang, 2016), the SJs operating with this L and VR combination generate hairpin vortices in the boundary layer, which are very close to the wall and hence are desirable for flow separation delay (Zhang and Zhong, 2010 and Zhong and Zhang, 2013). Furthermore, by varying the operational phase difference between the two SJ actuators, the interactions between the in-line twin SJs and the separated flow are investigated at various phase differences. Here the phase difference is defined as $\Delta\phi = \phi_u - \phi_d$, where ϕ_u and ϕ_d are the phases of the upstream SJ actuator and of the downstream one, respectively. Four different phase differences are investigated, i.e., $\Delta\phi = 0^\circ, 90^\circ, 180^\circ$, and 270° (or -90°).

C. Particle image velocimetry (PIV)

PIV measurements are conducted in two planes: one is the mid-span plane as shown in Fig. 2 and the other is a plane parallel to inclined Plate 3. Similar to the experiments in our previous studies (Wen *et al.*, 2015 and Wen and Tang, 2016), Dantec Dynamics polyamide seeding particles with a mean diameter of $20\ \mu\text{m}$ are used to track the water flow with high accuracy. A light sheet of approximately 2 mm thickness is generated by a 200 mJ double pulsed Nd:YAG laser to illuminate the seeding particles. A FlowSense 2M CCD camera with a Nikon 60 mm lens is used to capture a field of view of $x = -2D_o \sim 22D_o$ and $y = -3D_o \sim 6D_o$ in the mid-span plane. The corresponding vectors are resolved using a two-frame cross-correlation algorithm, in which a 32×32 pixel interrogation area (IA) with an overlap ratio of 50% is chosen, giving a 1.30 mm spatial separation between adjacent vectors. For the spanwise-wall-parallel PIV measurements, the light sheet is placed about 5 mm, i.e., $1D_o$, below inclined Plate 3 so as to keep the surface reflection at an acceptable level. The wall-parallel measurement is taken in a field of view of $x = 7D_o \sim 29D_o$ and $y = \pm 13D_o$, covering both the forward and backward flow portions of the separated flows. By using an IA of 32×32 pixels in two-frame cross-correlation algorithm, 1.50 mm spatial resolution is obtained. The overall relative error of the measured velocity components e_{total} is about 1% (Wen *et al.*, 2015).

The PIV system is controlled to shoot the laser at certain phases, which are defined according to the movement of the upstream actuator diaphragm, i.e., $t/T = 0$ (and 1), $1/4$, $1/2$, and $3/4$ correspond to the beginning of blowing, maximum blowing, beginning of ingestion, and maximum ingestion, respectively. Eight consecutive phases in one cycle are captured and analyzed in the present study. According to Jabbal and Zhong (2010), an average of 60 velocity vector images is sufficient for SJs in laminar flows. Since for the present study flow separation is involved, 100 pairs of images are used for phase averaging.

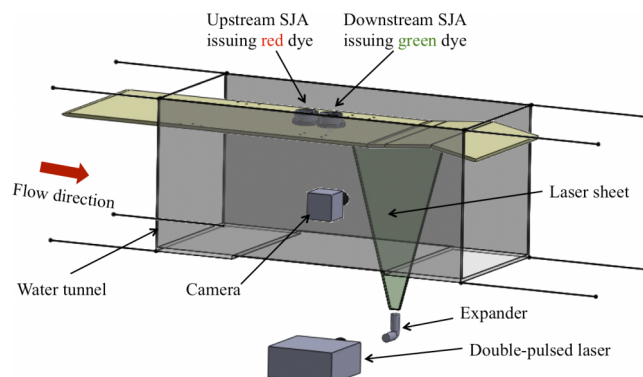


FIG. 2. Schematic of PIV measurement system.

D. Color dye visualization

To visualize the twin SJs in the attached and separated crossflows, food dye of two different colors is used. The upstream SJ actuator is filled with red dye and the downstream one filled with green dye. The dye is premixed with methanol to achieve a density very close to water's. In the experiment, a color high-speed camera (MotionBLITZ EoSens) operating at a frame rate of 60 fps is used to capture the dye pattern produced by the SJs from the side view.

E. POD analysis methods

The proper orthogonal decomposition (POD) analysis method, first introduced by Lumley (1967), is a useful tool for detection of energy-carrying, coherent flow structures embedded in unsteady flows. It has been widely applied to analyze unsteady characteristics of uncontrolled and controlled wakes shed by bluff bodies (Wu and Tang, 2014 and Ben Chiekh *et al.*, 2013) and of laminar separation bubbles (Lengani *et al.*, 2014). The principle and equations of POD can be found in many places in the literature and hence they are only briefly summarized below. In the present study, the “snapshot” POD method (Sirovich and Kirby, 1987) is implemented. In this POD, an unsteady velocity field $\mathbf{u}(\mathbf{x}, t)$ can be decomposed into the form of

$$\mathbf{u}(\mathbf{x}, t) = \bar{\mathbf{u}}(\mathbf{x}) + \mathbf{u}'(\mathbf{x}, t) = \bar{\mathbf{u}}(\mathbf{x}) + \sum_{n=1}^N a_n(t) \Phi_n(\mathbf{x}), \quad (1)$$

where $\bar{\mathbf{u}}(\mathbf{x})$ is the mean velocity field, $\mathbf{u}'(\mathbf{x}, t)$ the instantaneous fluctuating velocity field, $\Phi_n(\mathbf{x})$ the deterministic spatial POD modes, $a_n(t)$ the temporal coefficient corresponding to the n th POD mode, and N the number of snapshots used in the calculation. The temporal coefficients $a_n(t)$ are obtained by solving an eigenvalue problem associated with $\mathbf{u}'(\mathbf{x}, t)$

$$\lambda_n a_n(t_i) = \sum_{j=1}^N \left(\sum_{\mathbf{x}} \mathbf{u}'(\mathbf{x}, t_i) \cdot \mathbf{u}'(\mathbf{x}, t_j) \right) a_n(t_j), \quad (2)$$

where (\cdot) represents the inner product of two vectors. For snapshot POD, t_i and t_j in Eq. (2) indicate the i th and j th snapshots, respectively, instead of actual time. The eigenvalues λ_n are real and positive and form a decreasing and convergent series. The POD modes can then be calculated by

$$\Phi_n(\mathbf{x}) = \sum_{i=1}^N \mathbf{u}'(\mathbf{x}, t_i) a_n(t_i) \left/ \left\| \sum_{i=1}^N \mathbf{u}'(\mathbf{x}, t_i) a_n(t_i) \right\| \right., \quad (3)$$

where $\|\cdot\|$ is the discrete 2-norm.

A convergence study for the POD analysis is conducted. It is found that the discrepancy for the first five eigenvalues is within 5% if the number of snapshots is greater than 300. This indicates that the number of snapshots $N = 400$, which is used in the present study, is sufficient for providing statistically convergent results for at least the most energized POD modes.

III. RESULTS AND DISCUSSION

A. Interaction of the in-line twin SJs with the separated boundary layer

Our previous works (Wen *et al.*, 2015 and Wen and Tang, 2016) have revealed that in the same attached boundary layer hairpin vortices are produced by the single SJ (Fig. 3(a)), and three types of vortex structures are induced by the in-line twin SJs: *one combined vortex* at phase difference $\Delta\phi = 90^\circ$ where the two hairpin vortices interact in a very constructive way (Fig. 3(c)), *two completely separated hairpin vortices* at $\Delta\phi = 270^\circ$ where the two hairpin vortices hardly interact (Fig. 3(e)), and *partially interacting vortex structures* at $\Delta\phi = 0^\circ$ and 180° (Figs. 3(b) and 3(d)) where the head of one hairpin vortex is coupled with the legs of the other. In addition, vortices

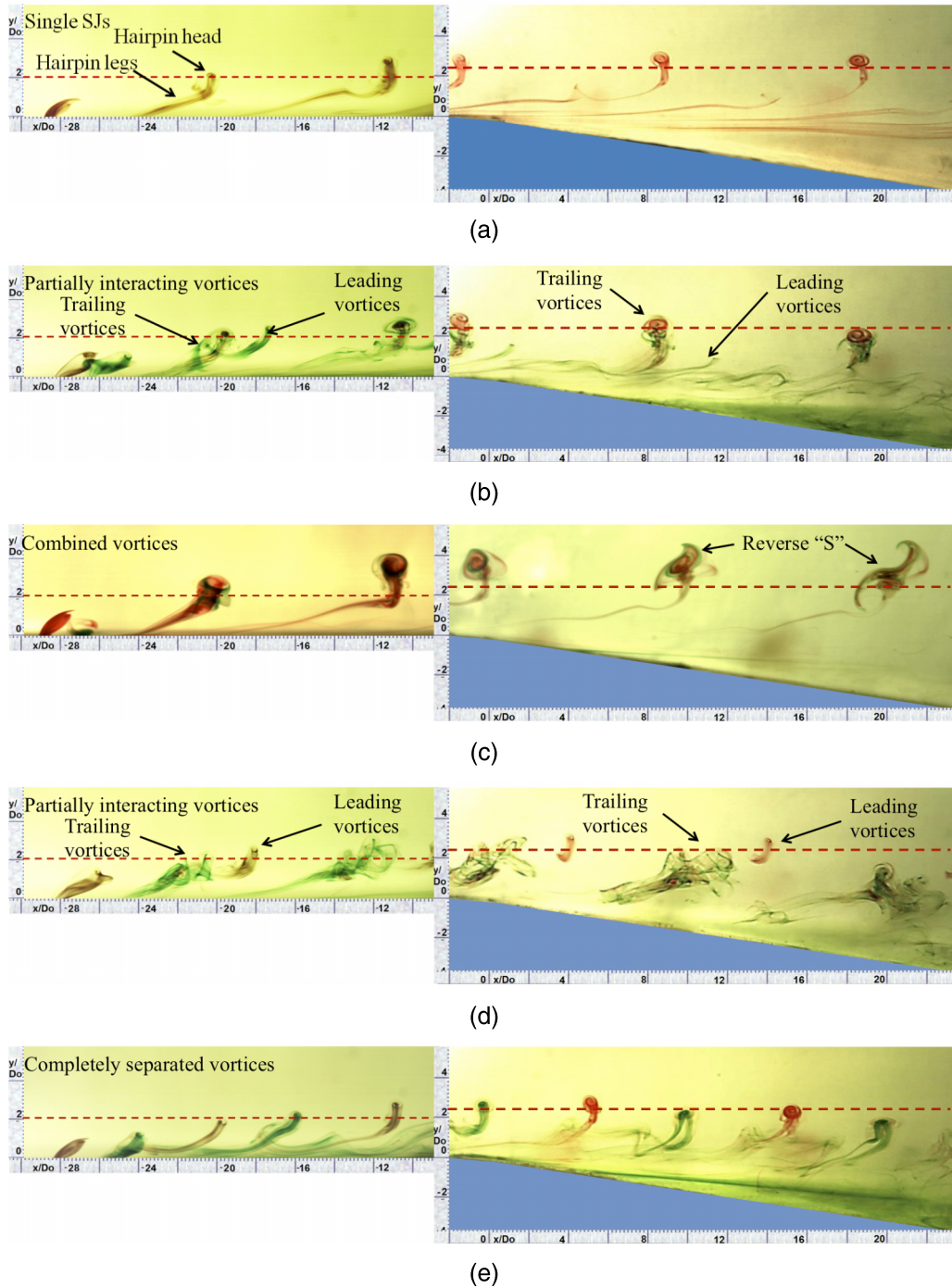


FIG. 3. Dye images of (a) the single SJ and (b)–(e) the in-line twin SJs at various phase differences in the attached boundary layer (left) and in the separated boundary layer (right). The dashed lines indicate the edge of the boundary layer at the inlet of each subfigure.

issued from the upstream actuator (in red) are more sustained than those from the downstream actuator (in green). When these vortex structures travel downstream and enter the separated boundary layer (as will be shown in Fig. 4(a), the boundary layer separates from the inclined wall at about $x = 4D_o$), it seems that they have lost their cross-stream momentum and no longer penetrate the boundary layer. Instead, due to the increase of flow cross-sectional area, they even travel towards the inclined wall.

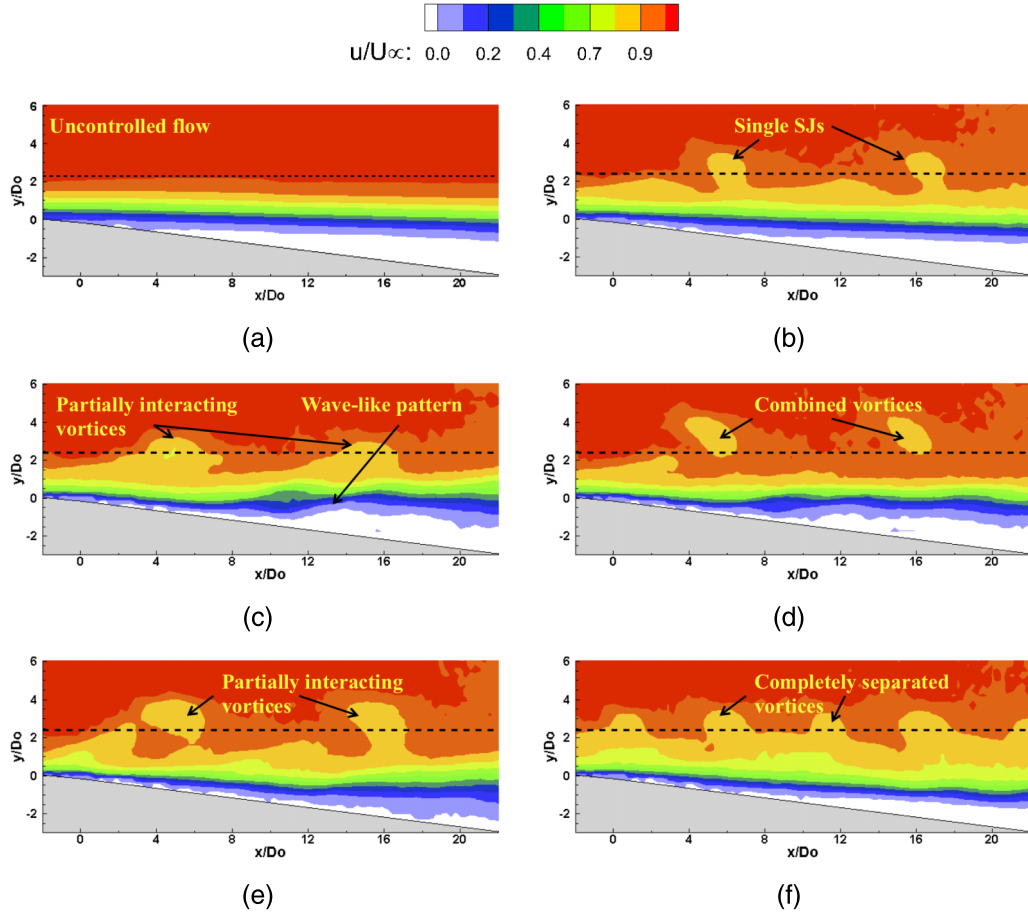


FIG. 4. Contours of (a) time-averaged and (b)–(f) phase-averaged streamwise velocity in the mid-span plane at $t/T = 0.2$.

In most of the cases, the heads of vortices that are produced from the upstream actuator (in red) do not change too much when compared to those in the attached boundary layer. An exception is the $\Delta\phi = 90^\circ$ case, in which the vortex head gradually loses its coherence and stretches out, showing a reversed letter “S” (see Fig. 3(c)). The vortex legs, however, are affected significantly by the separated flow because of their lower positions. Due to the large shear along the upper edge of the reversed flow region (defined by white regions of streamwise velocity contours in Fig. 4), all vortex legs are highly stretched. Furthermore, except for the $\Delta\phi = 90^\circ$ case where the one combined vortex is strong enough to escape, in the other cases there are more or less some dye being trapped in the reversed flow region, which is especially prominent in the $\Delta\phi = 0^\circ$ and 270° cases.

The PIV results not only capture the aforementioned vortex structures under different conditions but also reveal the extent of their influence on the separated boundary layer. Fig. 4 shows the contours of phase-averaged streamwise velocity in the mid-span plane for the same cases as in Fig. 3 (time-averaged for the uncontrolled case). To highlight the flow separation, the reversed flow regions (i.e., with negative streamwise velocity) are colored in white. As shown in Fig. 4(a), the undisturbed boundary layer starts to separate at about $x = 4D_o$, after which the separated flow gradually tilts towards the inclined wall. When the single SJ is applied, as shown in Fig. 4(b), the induced hairpin vortices appear as a sequence of low-speed lumps that travels downstream, the separation point is slightly pushed downstream to about $x = 6.5D_o$, and the separated flow tilts more towards the inclined wall.

When the twin SJs are applied, the low-speed lumps vary from case to case. At $\Delta\phi = 90^\circ$ where combined vortices are produced (Fig. 4(d)), the lumps are the farthest from the wall because these vortices are formed in a very constructive way and hence most penetrate the boundary layer during

their emergence. At $\Delta\phi = 270^\circ$ where completely separated hairpin vortices are produced (Fig. 4(f)), the lumps appear with a doubled wave number. At $\Delta\phi = 0^\circ$ and 180° where partially interacting vortex structures are produced (Figs. 4(c) and 4(e)), however, the lumps only represent the more sustained vortices produced from the upstream SJ actuator. The vortices produced from the downstream SJ actuator lose their coherence and are hence smoothed out in the phase averaging process.

From Fig. 4, it can also be seen that the periodic passage of low-speed lumps or vortex structures can influence the separated flow significantly. The unsteady, non-uniform flow right above the reversed flow region causes the flapping of the region's upper edge (the blue-white interface). It is believed that this flapping behavior results in the delay of flow separation. This is confirmed by the time-averaged results shown in Fig. 5. It is seen from Fig. 5(b) that, under the influence of the single SJ, the separation point is delayed a bit, from about $x = 4D_o$ to about $6D_o$. As a result, the area of the reversed flow region reduces. With the implementation of the twin SJs, the separation point is further pushed downstream regardless of the phase difference. The new separation points are located at about $x = 8D_o$, $10D_o$, $18D_o$, and $10D_o$ for the cases at $\Delta\phi = 0^\circ$, 90° , 180° , and 270° , respectively. It is surprising to see that the separated flow almost re-attaches to the wall at $\Delta\phi = 180^\circ$ (Fig. 5(e)), which is neither the case producing combined vortices nor the case producing completely separated hairpin vortices. The same control effect does not happen in the other partially interacting case at $\Delta\phi = 0^\circ$. This interesting finding is consistent to our previous finding in the attached flow under the same condition (Wen *et al.*, 2015): at $\Delta\phi = 180^\circ$ the twin SJs can induce the greatest near-wall velocity surplus in the mid-span plane. The greatest separation delay may be attributed to the trailing vortex structures as shown in Fig. 3(d). Although they seem to have lost their coherence, these vortex structures are quite close to the inclined wall and are hence able to exert more influence on the separated flow.

Since the SJ-induced vortex structures are very three dimensional, their influence on the separated flow is also examined in the wall-parallel plane, which is depicted by time-averaged streamwise velocity contours plus streamlines as shown in Fig. 6. These plan-view figures are displayed

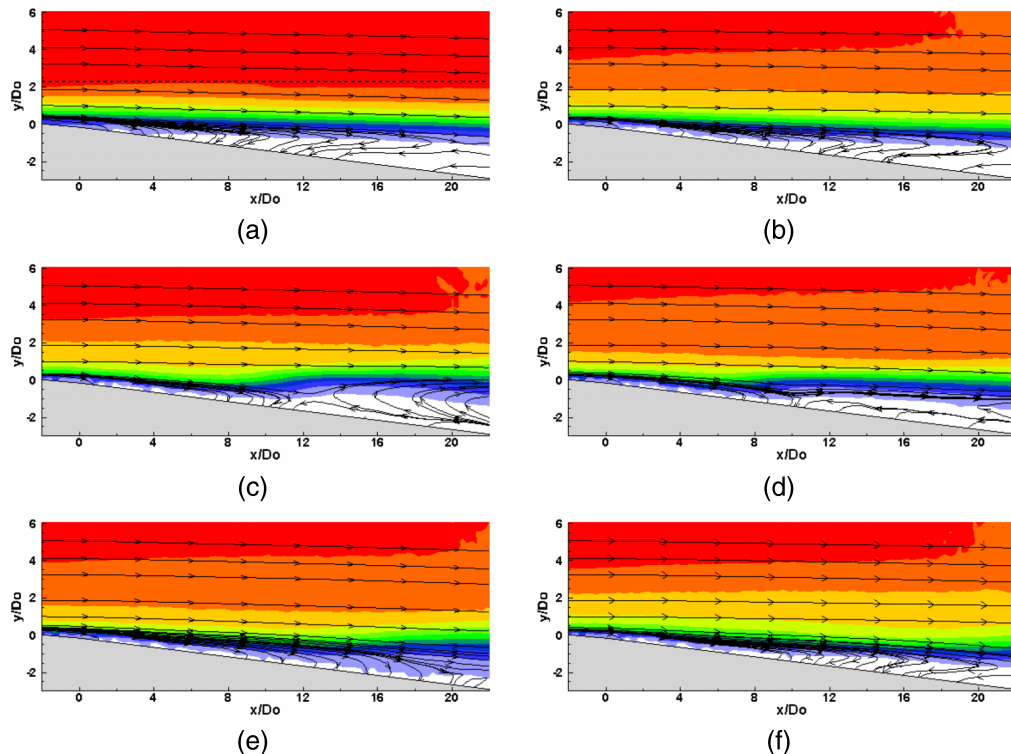


FIG. 5. Contours of time-averaged streamwise velocity and streamlines in the mid-span plane (refer to Fig. 4 for the color map).

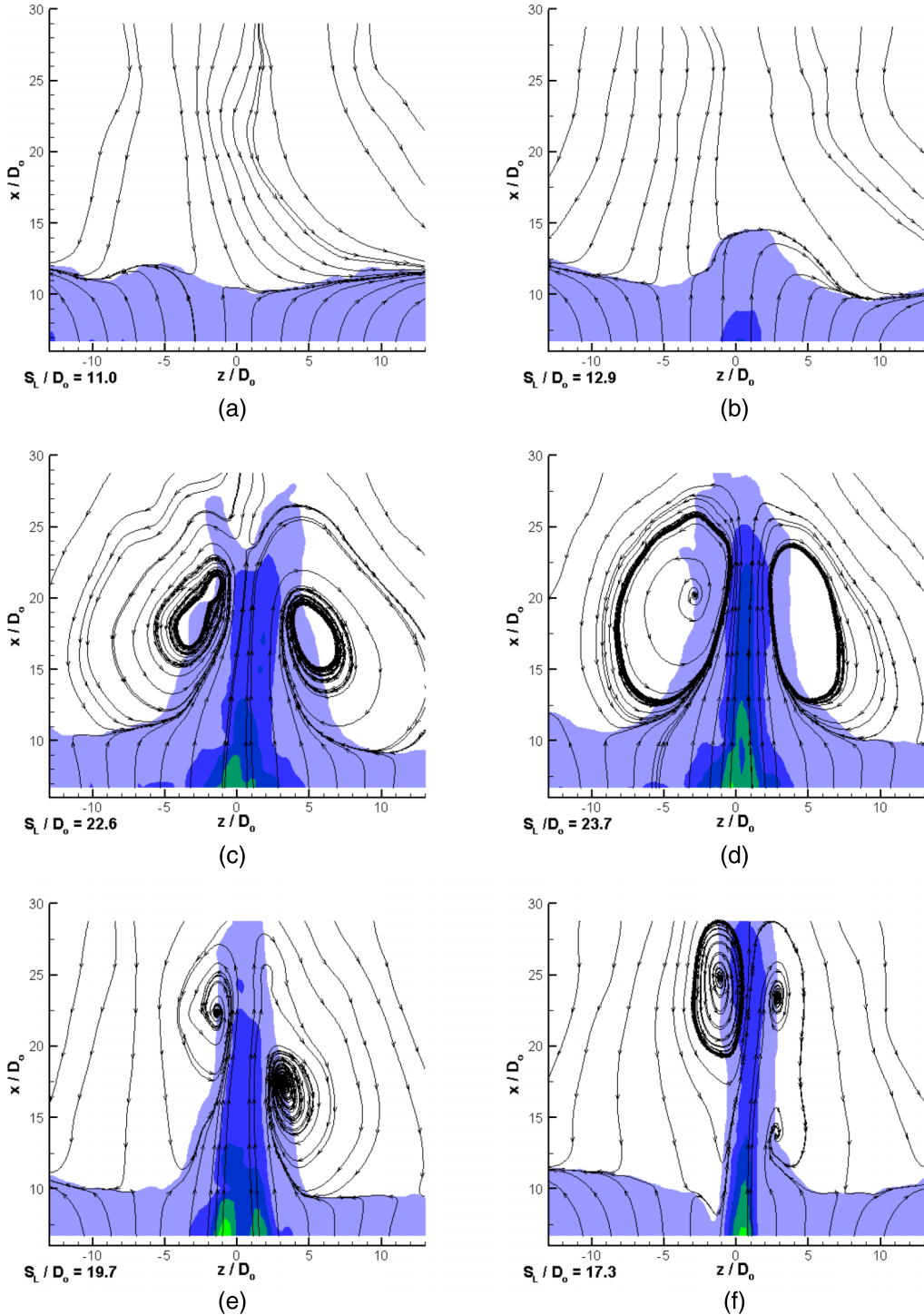


FIG. 6. Contour of time-averaged streamwise velocity superimposed by streamlines in the plane parallel to inclined Plate 3. S_L/D_o indicates the averaged separated line within $z = -5D_o$ to $5D_o$ (refer to Fig. 4 for the color map).

in such a way that the main stream flows from the bottom to the top. As shown in Fig. 6(a), the undisturbed separation line is roughly along the spanwise direction, which can be told either by the interface between the forward flow (lower blue colored region) and the reversed flow (upper white region) or by the spanwise streamlines. Furthermore, to compare the control effect, a quantity, S_L , is introduced to describe the mean streamwise location of the separation line over a spanwise range

$z = -5D_o$ to $5D_o$, within which the most influence of the SJs is exerted. Since the measurement plane is about $1D_o$ away from the inclined wall, in the uncontrolled case $S_L = 11.0D_o$.

When the single SJ is introduced, a slight protrusion of the forward flow is observed near the mid-span line in Fig. 6(b), indicating the separation delay with the mean separation line being slightly pushed downstream to $S_L = 12.9D_o$. This protrusion becomes more obvious when the in-line twin SJs are applied, regardless of their phase difference. At all four phase differences, a prominent forward-flow streak appears along the mid-span line, beside which a pair of recirculation zones is induced. The strongest streak is observed at $\Delta\phi = 90^\circ$, which spans about $8D_o$ and protrudes up to about $28D_o$. It is also accompanied by the largest recirculation zones (Fig. 6(d)). In this case, the mean streamwise location of the separation line is $S_L = 23.7D_o$, delayed for a distance of $12.7D_o$. The forward-flow streak is slimmest at $\Delta\phi = 270^\circ$ as shown in Fig. 6(f), spanning only about $5D_o$. But it lasts for the longest distance, even reaching out of the upper boundary ($x = 29D_o$) of the current measurement field of view. Based on this cutoff distance ($x = 29D_o$), the mean streamwise location of the separation line in this case is evaluated as $S_L = 17.3D_o$, much smaller than in the $\Delta\phi = 90^\circ$ case due to the much slimmer streak. This is not surprising because our previous study in the attached boundary layer has revealed the reason (Wen *et al.*, 2015). The combined vortices together with their accompanying vortices at $\Delta\phi = 90^\circ$ exert the greatest spanwise impact on the near-wall flow, but as they quickly penetrate the boundary layer the impact vanishes. On the contrary, the two completely separated hairpin vortices and their accompanying vortices at $\Delta\phi = 270^\circ$ only affect the near-wall flow in a narrow band around the mid-span plane like what the single SJ does, but they stay low in the boundary layer and hence maintain their influence for quite a long distance.

At $\Delta\phi = 180^\circ$ where partially interacting vortex structures are produced, as shown in Fig. 6(e), the controlled flow shows an intermediate pattern, i.e., with a streak slimmer but longer than that in the $\Delta\phi = 90^\circ$ case, and wider but shorter than that in the $\Delta\phi = 270^\circ$ case. The mean streamwise location of the separation line in this case is evaluated as $S_L = 19.7D_o$, also between the values of the other two cases. Surprisingly, in another partial interacting case at $\Delta\phi = 0^\circ$, as shown in Fig. 6(c), the streak is even wider but shorter than that in the $\Delta\phi = 90^\circ$ case, and the mean location of the separation line is $S_L = 22.6D_o$. The significant difference between these two partial interacting cases stems from the large difference of the trailing vortices that are close to the inclined wall. In the $\Delta\phi = 0^\circ$ case, as shown in Fig. 3(b), the trailing vortices mainly consist of the hairpin vortices produced from the upstream SJ actuator (in red), which are able to sustain their coherence for quite a long time. Hence the trailing vortices enhance their strength by entraining the leading hairpin legs and behave somehow like the combined vortices as in the $\Delta\phi = 90^\circ$ case. On the other hand, in the $\Delta\phi = 180^\circ$ case as shown in Fig. 3(d), the trailing vortices mainly consist of the hairpin vortices produced from the downstream SJ actuator (in green), which lose their coherence soon after their emergence. Although they also entrain the leading hairpin legs, their streak appearing in the wall-parallel plane falls between those in the $\Delta\phi = 90^\circ$ and 270° cases.

B. POD analysis

As revealed in Sec. III A, the single or twin SJs interact with the separated flow in a dynamic way, involving periodic passage of the vortex structures and flapping of the separated boundary layer. POD analysis is then implemented in the mid-span plane to extract energy-carrying coherent structures from the flow field. For the single SJ case, the fractional contributions of the first ten POD modes to the total fluctuation kinetic energy, $\lambda_n/\Sigma\lambda_n$, are plotted in Fig. 7(a). Although all less than 10% due to the relatively weak single SJ vortices and non-negligible noise in the background flow, the energy levels of the first three modes still stand out from the rest modes. In the first mode Φ_1 , the energy level is 5.7%, slightly higher than those of the next two modes. As revealed in Fig. 7(b), a strip of back-and-forth fluctuation flow is captured in this mode along the upper edge of the reversed flow, which grows its size and magnitude in the streamwise direction. This type of fluctuation also appears in the POD analysis results of various shear-layer flows, where the fluctuation amplification is attributed to auto-generated shedding vortices, i.e., the Kelvin-Helmholtz vortices (Simoni *et al.*, 2013 and Lengani *et al.*, 2014). In the present flow, however, since the same mode is not found in

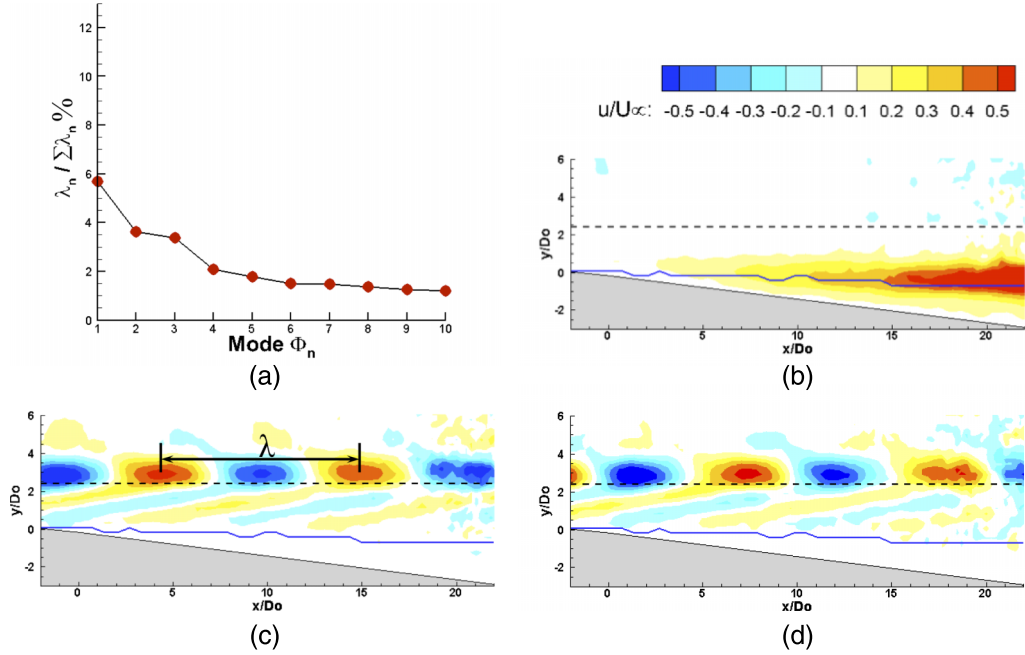


FIG. 7. POD analysis for the single SJ case in the mid-span plane: (a) POD energy levels of the first 10 modes and (b)–(d) contours of streamwise velocity of the first 3 POD modes. The black dashed line indicates the edge of the boundary layer at $x=0$, and the blue solid line represents the upper edge of the reversed flow.

the uncontrolled case, it is believed that the fluctuation strip is induced and amplified by the periodic passage of SJ-induced vortex structures.

The next two POD modes, Φ_2 and Φ_3 , appear in pair, and their energy levels (i.e., 3.6% and 3.4%, respectively) are close. As shown in Figs. 7(c) and 7(d), this pair of modes has very similar

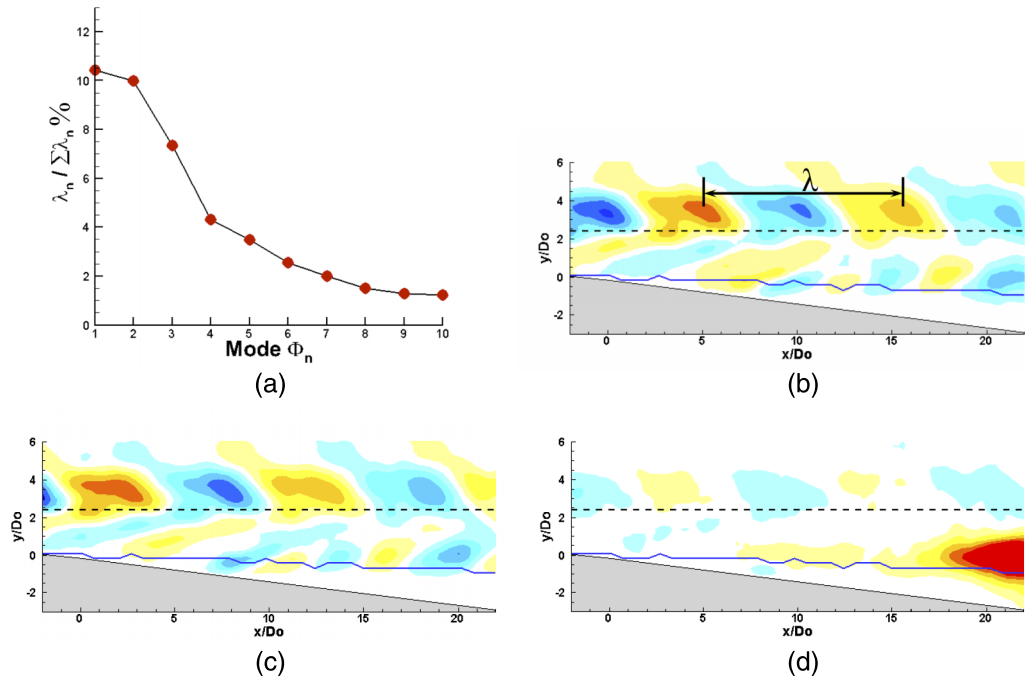


FIG. 8. POD analysis for the $\Delta\phi = 90^\circ$ case in the mid-span plane: (a) POD energy levels of the first 10 modes and (b)–(d) contours of streamwise velocity of the first 3 POD modes (refer to Fig. 7 for the color map).

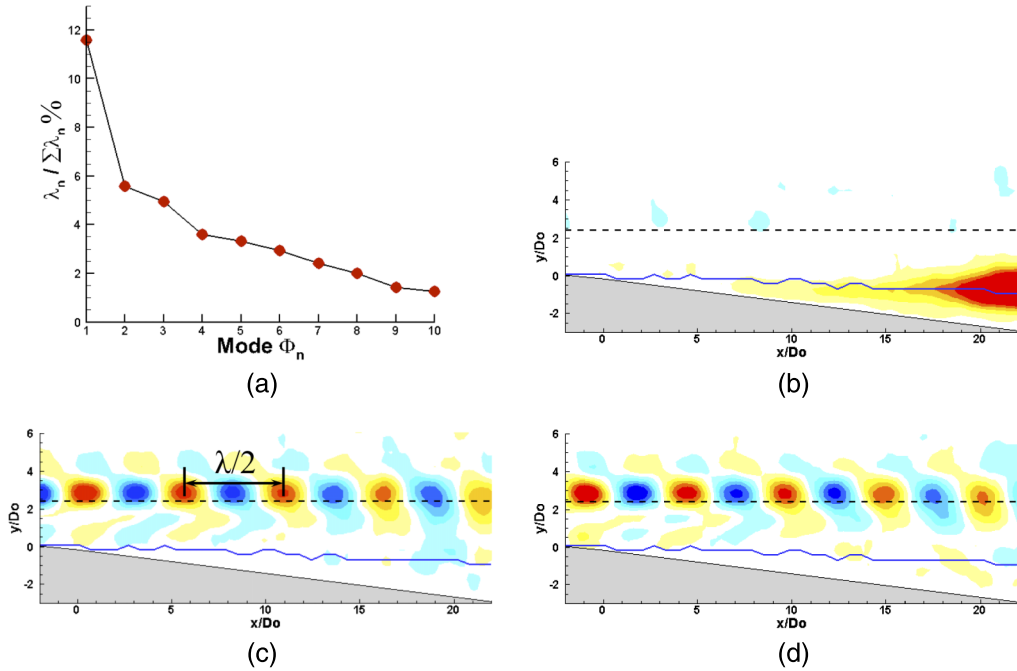


FIG. 9. POD analysis for the $\Delta\phi = 270^\circ$ case in the mid-span plane: (a) POD energy levels of the first 10 modes and (b)–(d) contours of streamwise velocity of the first 3 POD modes (refer to Fig. 7 for the color map).

flow structures, i.e., lumps of forward and backward flows appearing alternatively along the edge of the boundary layer, with a spatial shift of about $1/4$ wavelength. This reveals the convective nature of these flow structures. By comparing the location and wavelength of these flow structures with the phase-averaged results shown in Fig. 4(b), it is confirmed that this mode pair captures the convection of the single-SJ induced hairpin vortices.

As the twin SJs operate at $\Delta\phi = 90^\circ$ and generate combined hairpin vortices, the sequence of the first three POD modes changes: now the convective mode pair (Φ_1 and Φ_2) leads the mode sequence whereas the back-and-forth fluctuation along the upper edge of the reversed flow becomes the third mode (Φ_3). The energy levels of the convective mode pair (10.4% and 10.0%) are almost tripled compared to those in the single SJ case. The corresponding coherent structures shown in Figs. 8(b) and 8(c) are located significantly beyond the edge of the boundary layer because of their enhanced strength. The third mode, Φ_3 , increases its energy contribution too, from 5.7% to 7.3%. Its corresponding strip of back-and-forth fluctuation flow becomes wider and is located further downstream, as shown in Fig. 8(d).

As the twin SJs operate at $\Delta\phi = 270^\circ$ and generate two completely separated hairpin vortices, the sequence of the first three POD modes becomes the same as in the single SJ case, and the energy levels of these modes all increase. The first mode Φ_1 contributes about 11.6% of the overall fluctuation energy, indicating that the reversed flow is more efficiently influenced in this case. The corresponding strip of back-and-forth fluctuation flow is wider and much closer to the inclined plate as shown in Fig. 9(b). As a result, the separated flow can be more effectively delayed than in the previous two cases (see Fig. 5). The mode pair, Φ_2 and Φ_3 , contributes about 5.6% and 4.9% of the overall fluctuation energy. As shown in Figs. 9(c) and 9(d), this mode pair presents the convection of a doubled number of flow structures, resulting in a half of the wavelength.

IV. CONCLUSIONS

An experimental investigation is carried out to investigate the interaction of in-line twin SJs with a separated laminar boundary layer flow over inclined plates. The flow structures issued by the

twin SJs at four phase differences are visualized and compared in the separated flow. The extent of the flow separation delay caused by these flow structures is also examined using PIV measurement in two planes. The most energetic coherent structures in the flow are extracted from the PIV data using the POD analysis. The main findings from this study are summarized as follows:

- (i) The dye visualization shows that, when entering the separated boundary layer, all the twin SJ produced vortex structures travel towards the inclined wall. In most of the cases, the heads of vortices that are produced from the upstream SJ actuator do not change too much, and the vortex legs are highly stretched by the separated shear layer. An exception is the $\Delta\phi = 90^\circ$ case where the combined vortex head appears as a reversed letter “S” and the combined vortex legs are high enough to escape from the influence of the separated flow.
- (ii) Compared to the single SJ, the twin SJs exert stronger influence on the separated flow regardless of the phase difference. The PIV results in the mid-span plane reveal that the periodic passage of vortex structures influences the separated flow significantly, causing the flapping of the upper edge of the reversed flow region. This flapping behavior results in the delay of flow separation. It is interesting to see that, among the four phase differences, at $\Delta\phi = 180^\circ$ the separated flow almost re-attaches to the wall, which can be attributed to the influence of very-close-to-wall trailing vortex structures.
- (iii) The delay of separation is demonstrated by a streak of forward flow protrusion in the wall-parallel PIV results. At $\Delta\phi = 90^\circ$ where combined vortices are produced, the streak is wide and short, whereas at $\Delta\phi = 270^\circ$ where fully separated hairpin vortices are produced, the streak is slim and long. The delay effect also differs for the other two cases producing partially interacting vortex structures: at $\Delta\phi = 180^\circ$, the streak shows an intermediate pattern of the previous two cases, but at $\Delta\phi = 0^\circ$, the streak is even wider and shorter than that in the $\Delta\phi = 90^\circ$ case.
- (iv) The POD analysis in the mid-span plane identifies two major types of energetic flow structures in the controlled flow: a strip of back-and-forth fluctuation along the upper edge of the reversed flow, and the vortex structures produced by the twin SJs. The former structures are associated with the shear-layer flow subject to the influence of periodic passage of SJ-induced vortex structures, whereas the latter structures come with a mode pair demonstrating a convective phenomenon. It is found that the energy contribution of these two types of flow structures in the twin SJ cases is generally larger than that in the single SJ case. The fluctuation strip is most energetic in the single SJ case and the $\Delta\phi = 270^\circ$ case, whereas the convective mode pair is most energetic in the $\Delta\phi = 90^\circ$ case.

This investigation improves our understanding in the interaction of in-line twin SJs in a separated laminar boundary layer, which is useful for future SJ-array applications.

ACKNOWLEDGMENTS

The first author of this paper, Dr. Xin Wen, would like to acknowledge the financial support from Nanyang Technological University for his Ph.D. study.

- Amitay, M. and Glezer, A., “Role of actuation frequency in controlled flow reattachment over a stalled airfoil,” *AIAA J.* **40**(2), 209–216 (2002).
- Ben Chiekh, M., Michar, M., Guellouz, M. S., and Béra, J. C., “POD analysis of momentumless trailing edge wake using synthetic jet actuation,” *Exp. Therm. Fluid Sci.* **46**, 89–102 (2013).
- Crook, A. and Wood, N. J., “Measurements and visualizations of synthetic jets,” AIAA Paper 2001–0145, 2001.
- Dandois, J., Garnier, E., and Sagaut, P., “Numerical simulation of active separation control by a synthetic jet,” *J. Fluid Mech.* **574**, 25 (2007).
- Glezer, A. and Amitay, M., “Synthetic jets,” *Annu. Rev. Fluid Mech.* **34**, 503–529 (2002).
- Honami, S. and Motosuke, M., “Vortex interaction of in-line synthetic jets injected at different phase in low Reynolds number cross flow,” AIAA Paper 2012–3243, 2012.
- Iai, T., Motosuke, M., and Honami, S., “Vortex behavior of vertical and inclined synthetic jet in cross flow at low Reynolds number,” AIAA Paper 2009–4178, 2009.
- Ibrahim, I. H. and Skote, M., “Simulations of the linear plasma synthetic jet actuator utilizing a modified Suzen-Huang model,” *Phys. Fluids* **24**, 113602 (2012).
- Jabbal, M. and Zhong, S., “The near wall effect of synthetic jets in a boundary layer,” *Int. J. Heat Fluid Flow* **29**(1), 119–130 (2008).

- Jabbal, M. and Zhong, S., "Particle image velocimetry measurements of the interaction of synthetic jets with a zero-pressure gradient laminar boundary layer," *Phys. Fluids* **22**(6), 063603 (2010).
- Lengani, D., Simoni, D., Ubaldi, M., and Zunino, P., "POD analysis of the unsteady behavior of a laminar separation bubble," *Exp. Therm. Fluid Sci.* **58**, 70–79 (2014).
- Liddle, S. C., Crowther, W. J., and Wood, N. J., "Investigation of phase and spacing effects in synthetic jet actuator arrays," AIAA Paper 2005-107, 2005.
- Liddle, S. C. and Wood, N. J., "Investigation into clustering of synthetic jet actuators for flow separation control application," *Aeronaut. J.* **109**, 35–44 (2005).
- Lumley, J. L., "The structure of inhomogeneous turbulent flow," in *Atmospheric Turbulence and Radio Wave Propagation* (Nauka, Moscow, 1967), pp. 166–178.
- Schaeffler, N. W. and Jenkin, L. N., "Isolated synthetic jet in crossflow: Experimental protocols for a validation dataset," *AIAA J.* **44**, 2846–2856 (2006).
- Simoni, D., Ubaldi, M., and Zunino, P., "Experimental investigation of the interaction between incoming wakes and instability mechanisms in a laminar separation bubble," *Exp. Therm. Fluid Sci.* **50**, 54–60 (2013).
- Sirovich, L. and Kirby, M., "Low-dimensional procedure for the characterization of human faces," *J. Opt. Soc. Am. A* **4**(3), 519–524 (1987).
- Tang, H., Salunkhe, P., Zheng, Y., Du, J., and Wu, Y., "On the use of synthetic jet actuator arrays for active flow separation control," *Exp. Therm. Fluid Sci.* **57**, 1–10 (2014).
- Watson, M., Jaworski, A. J., and Wood, N. J., "Contribution to the understanding of flow interactions between multiple synthetic jets," *AIAA J.* **41**, 747–749 (2003).
- Wen, X. and Tang, H., "On hairpin vortices induced by circular synthetic jets in laminar and turbulent boundary layers," *Comput. Fluids* **95**, 1–18 (2014).
- Wen, X. and Tang, H., "Effect of phase difference on the interaction of hairpin vortices induced by in-line twin synthetic jets," *J. Visualization* **19**(1), 79–87 (2016).
- Wen, X., Tang, H., and Duan, F., "Vortex dynamics of in-line twin synthetic jets in a laminar boundary layer," *Phys. Fluids* **27**(8), 083601 (2015).
- Wu, Y. and Tang, H., "POD study of a turbulent boundary layer over a rough forward-facing step," in *Fluid-Structure-Sound Interactions and Control*, edited by Zhou, Y., Liu, Y., Huang, L., and Hodges, D. H. (Springer, Berlin, 2014), pp. 83–88.
- Zaman, K. B. M. Q. and Milanovic, I. M., "Synthetic jets in cross-flow. Part 1. Round jet," AIAA Paper 2003-3714 (2003).
- Zhang, S. and Zhong, S., "Experimental investigation of flow separation control using an array of synthetic jets," *AIAA J.* **48**(3), 611–623 (2010).
- Zhong, S., Jabbal, M., Tang, H., Garcillan, L., Guo, F., Wood, N., and Warsop, C., "Towards the design of synthetic-jet actuators for full-scale flight conditions," *Flow, Turbul. Combust.* **78**(3-4), 283–307 (2007).
- Zhong, S. and Zhang, S., "Further examination of the mechanism of round synthetic jets in delaying turbulent flow separation," *Flow, Turbul. Combust.* **91**(1), 177–208 (2013).